Water clusters: Untangling the mysteries of the liquid, one molecule at a time

Frank N. Keutsch* and Richard J. Saykally†

Department of Chemistry, University of California, Berkeley, CA 94720-1460

This contribution is part of the special series of Inaugural Articles by members of the National Academy of Sciences elected on April 27, 1999.

Contributed by Richard J. Saykally, May 29, 2001

Extensive terahertz laser vibration-rotation-tunneling spectra and mid-IR laser spectra have been compiled for several isotopomers of small (dimer through hexamer) water clusters. These data, in conjunction with new theoretical advances, quantify the structures, force fields, dipole moments, and hydrogen bond rearrangement dynamics in these clusters. This new information permits us to systematically untangle the intricacies associated with cooperative hydrogen bonding and promises to lead to a more complete molecular description of the liquid and solid phases of water, including an accurate universal force field.

The quest to achieve an accurate description of liquid water has produced major advances in the last two decades (1), yet despite the construction of hundreds of model force fields for use in simulations, the great advances in computational technology, and the development of powerful *ab initio* molecular dynamics methods, we remain unable to accurately calculate the properties of liquid water (e.g., heat capacity, density, dielectric constant, compressibility) over significant ranges in conditions (2). We do not yet have a satisfactory molecular description of how a proton moves in the liquid, we do not fully understand the molecular nature of the surfaces of either ice or liquid water (3), nor do we understand the origin of the intriguing anomalies and singularities found in the deeply supercooled region (4). Although it is clear that the hydrogen bond network and its fluctuations and rearrangement dynamics determine the properties of the liquid, no experimental studies exist that reveal detailed information on a molecular level without considerable interpretation (5). Moreover, the reliability of water models for simulating solvation phenomena and biological processes remains relatively untested.

A principal obstacle to resolving these issues is that of correctly describing the many-body, or cooperative nature of the hydrogen bonding interactions among a collection of water molecules. Theoretical work has shown that the H-bond is dominated by electrostatic interactions, balanced by the repulsive electron exchange, but that dispersion makes an appreciable contribution, whereas induction (polarization) is the dominant many-body effect (6, 7). It has proven notoriously difficult to accurately parameterize these interactions from *ab initio* calculations. Moreover, the *ab initio* molecular dynamics methods are based on density functional methods that explicitly omit the dispersion, and its expense mandates rather small sample sizes (e.g., 64 molecules) in simulations (8). But perhaps the central obstacle to developing quantitatively accurate and general methods has simply been the lack of a suitably precise data set with which to test and calibrate theoretical approaches.

The central goal of the research reviewed below is to advance the cause for accurately describing water in all its phases over arbitrarily large ranges of conditions, and the central contribution of our group has been to develop and apply novel methods of laser spectroscopy for the highly detailed study of water clusters to provide such a data set. Recently, we also have initiated studies of the hydrogen bond breaking dynamics in water clusters and comparison of them with mechanisms proposed to prevail in liquid water.

Terahertz Laser Vibration-Rotation-Tunneling (VRT) Spectroscopy of Clusters

The first far-IR (FIR) spectra of gaseous water clusters were measured near 22 cm^{-1} (455 μm) by Busarow *et al.* in 1989 (9). The spectra consisted of 56 $K_a = 2 \leftarrow 1$ rotation-tunneling transitions of $(H_2O)_2$, which complemented the microwave data (10, 11) obtained by the pioneering work of Dyke *et al.* (10), in obtaining an accurate description of the dimer ground state. Zwart *et al.* (12) subsequently extended these data to other quantum states. After some important technical developments that extended the operating range of the spectrometer to higher frequencies, Pugliano and Saykally (13) first measured an intermolecular VRT spectrum of a water cluster in 1992, with the detection of a torsional vibration of the D_2O trimer near 89.5 cm^{-1} (112 μm) (Fig. 1) (14–16). This striking spectrum exhibited an exact symmetric rotor pattern, and every rotational line was split into a distinctive quartet pattern that we now know results from quantum tunneling via two different hydrogen bond pathways connecting 48 degenerate minima on the 12-dimensional intermolecular potential surface. Pugliano *et al.* (17) quickly followed with the first observation of a dimer intermolecular vibration (acceptor twist), near 83 cm^{-1} (120 μm).

Subsequent work at Berkeley by Liu *et al.* (18) produced much more extensive trimer spectra and the first detailed assignment of the transitions. Cruzan *et al.* (19) discovered VRT spectra of the tetramer shortly afterward, and Liu *et al.* followed with the detection of the pentamer (20) and hexamer (21). Recent efforts have produced highly detailed characterizations of both the dimer and trimer, as well as greatly expanded data for the other clusters (22–27). We describe the current understanding of the dimer through hexamer clusters that has been achieved from these data, and through the efforts of many concurrent theoretical studies, in a later section.

IR Cavity Ringdown Spectroscopy

While mid-IR spectra of water clusters had been observed by the Pimentel group in matrix studies in 1957 (28), the OH stretching vibrations of gaseous water clusters were first studied indirectly in 1982 by Vernon *et al.* (29) in IR predissociation experiments in supersonic beams, and shortly after that by Page *et al.* (30). Vernon *et al.* assigned the spectra to $(H_2O)_n$, n = 1–5, and recorded a narrow transitions (15 cm^{-1}) at 3,715 cm^{-1}, which they attributed to the free OH stretch in cyclic water clusters, and a much broader feature (200 cm^{-1}) at lower frequency that they attributed to the bound OH stretch. Page *et al.* concentrated on the water dimer, finding four peaks, including the bound OH stretch, a broad transition at 3,545 cm^{-1}, red-shifted from the free monomer OH stretches. Coker *et al.* (31) found four dimer OH stretch frequencies identical to those determined by Page

Abbreviations: VRT, vibration-rotation-tunneling; FIR, far-IR; ASP, anisotropic site potential; IPS, intermolecular potential surface.

*Present address: Department of Chemistry and Chemical Biology, Harvard University, Cambridge, MA 02138.

†To whom reprint requests should be addressed. E-mail: saykally@uclink4.berkeley.edu.

CHEMISTRY

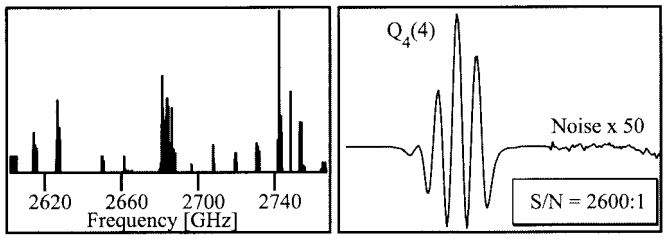

Fig. 1. The 89.5 cm^{-1} torsional hot band of $(D_2O)_3$ (*Left*) was the first intermolecular vibrational band observed for a water cluster in the gas phase (13). The spectrum shows splitting of each vibration-rotation transition into a characteristic quartet by the bifurcation tunneling motion (see Fig. 6*b*). (*Right*) Shown is this quartet for the 41.1 cm^{-1} torsional band (103), the most intense water trimer band observed to date. The intensities of the quartet components are determined by nuclear spin weights. S/N, Signal to noise.

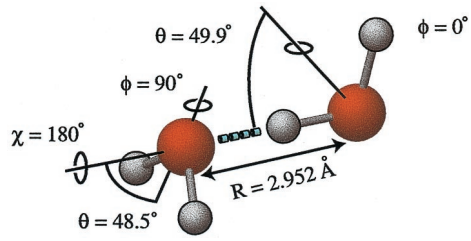

Fig. 3. The equilibrium structure of the water dimer as determined by calculations on the VRT(ASP-W)-II potential surface (R. S. Fellers, M. G. Brown, L. B. Braly, M. Colvin, C. Leforestier, and R.J.S., unpublished work). The hydrogen bond deviates 2.3° from linearity, the O—O distance is 2.952 Å, and the bond strength, D_0, is 3.40 kcal/mol. The highly nonrigid dimer has six floppy intermolecular vibrations.

et al. and also identified larger clusters in supersonic expansions carrying increasing concentrations of water. Huang and Miller (32, 33) reported the first rotationally resolved spectrum of $(H_2O)_2$ and observed the four OH stretch vibrations, and recently Frochtenicht *et al.* (34) used a size selection technique in which a He beam is used to eject clusters from a molecular beam as a function of their size. They were able to measure the free and bound OH stretching frequencies for clusters up to the pentamer.

The wide tuning range of our IR cavity ringdown laser absorption spectrometer recently permitted the first detailed studies of both the covalent bending vibrations of H_2O clusters (35), which occur near 1,600 cm^{-1}, and the stretching vibrations of D_2O clusters (36, 37), which fall near 2,700 cm^{-1} (Fig. 2). All of the observed clusters except the dimer exhibit strong vibrational predissociation broadening of their OD stretch spectra that obscures rotation-tunneling features. For the D_2O dimer, however, the acceptor antisymmetric stretch exhibits well-resolved acceptor switching doublets for each rotational line, whereas the donor stretch exhibits rotational lines that are broadened, but by about 30 times less than found for the H_2O isotopomer (36, 37). All bands observed for the cluster HOH bending vibrations are severely broadened, implying a stronger coupling with the dissociation coordinate (35). The sharp rotation-tunneling structure measured for $(D_2O)_2$ (Fig. 2*b*) was important for the determination of the dimer potential surface (38, 39), because the acceptor switching splittings cannot be

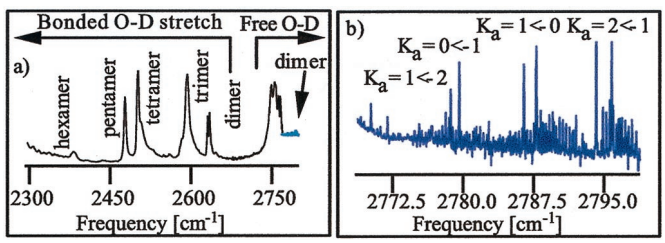

Fig. 2. The IR-cavity ringdown laser absorption spectrometer spectrum of the OD stretch region of D_2O is shown (*a*). The spectrum shows vibrational bands due to the stretch of the free OD at the highest frequencies. Below 2,700 cm^{-1} the OD stretch frequencies of the bound OD groups are observed on top of a weak broad absorption from an amorphous ice-like phase. The bound OD stretch frequencies decrease with increasing cluster size (40). The IR-cavity ringdown laser absorption spectrometer spectrum of the $(D_2O)_2$ acceptor antisymmetric OD stretch (*b*) shows the clearly resolved acceptor switching splitting. This splitting is most readily observable in the intense Q-branch transitions (36). This observation has allowed the determination of the acceptor switching splitting in the vibrational ground state, which was not possible with the previously existing data.

determined directly in the FIR experiments because of prohibitive selection rules. With the use of theoretical integrated band intensities, these cavity ringdown measurements permitted the first determination of the absolute water cluster concentrations in a supersonic beam (40). Interestingly, the trimer dominates the cluster distribution for both H_2O and D_2O. This domination is probably caused by the discontinuous increase in the per-monomer binding energy (D_0), which jumps from $1/2\ D_0$ to D_0 from dimer to trimer, while increasing much more slowly for larger clusters.

The Evolution of Hydrogen Bonding in Small Water Clusters

The archetype of the H-bond in water is the water dimer (Fig. 3). The O—O distance, reflecting the length of the H-bond is

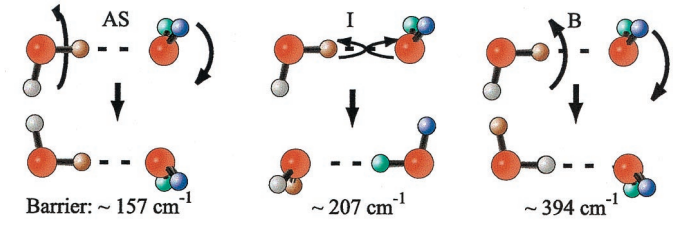

Fig. 4. The water dimer exhibits three distinct low barrier tunneling pathways that rearrange the hydrogen bonding pattern. Acceptor switching (AS), having the lowest barrier of all tunneling motions estimated at 157 cm^{-1} by VRT(ASP-W), is the most facile tunneling motion. This tunneling pathway exchanges the two protons in the hydrogen bond acceptor monomer and has been determined to begin with a flip of the acceptor monomer followed by a rotation of the donor monomer around its donating O—H bond, and completed by a 180° rotation of the complex about the O—O bond. The tunneling motion splits each rovibrational energy level into two. Interchange tunneling (I) exchanges the roles of the hydrogen bond donating and accepting water monomers. Several possible pathways exist for this exchange, the lowest barrier path being the geared interchange motion. This pathway begins with a rotation of the donor in the θ_D angle and rotation of the acceptor about its C_2 axis to form a trans transition state structure. This is followed by a rotation of the initial donor about its C_2 axis and a rotation of the initial acceptor in the θ_A angle such that it becomes the donor. The pathway is completed by a 180° end-over-end rotation of the complex. Calculations with the VRT(ASP-W) potential determine the barrier to be 207 cm^{-1}. The anti-geared interchange pathway also has been determined to be important and is similar to the geared pathway except that it has a cis transition state. The tunneling motion splits each energy level by a much smaller amount than the acceptor switching resulting into two sets of three energy levels. The bifurcation tunneling motion B, wherein the hydrogen bond donor exchanges its protons, consists of the simultaneous in plane librational motion of the donor with the flip of the acceptor monomer. This is the highest barrier tunneling pathway [394 cm^{-1} with VRT(ASP-W)] resulting in a small shift of the energy levels.

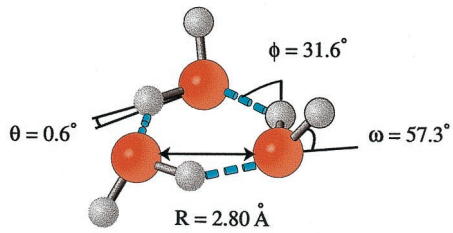

Fig. 5. The water trimer has a chiral cyclic equilibrium structure with each water monomer acting as a single hydrogen bond donor and acceptor (75, 98). It is homodromic in the sense that the donor OH bonds all are directed in a clockwise or anticlockwise pattern. The free hydrogens lie alternatingly above and below the plane of the oxygen atoms. This results in two adjacent free hydrogens being on the same side of the ring, making the trimer a frustrated structure, which gives rise to very facile torsional motions. These vibrationally average the structure to that of an oblate symmetric top on the experimental time scale. The average O—O distance of 2.85 Å [2.80-Å equilibrium *ab initio* value (105)] is significantly shorter than that of the water dimer, which can largely be attributed to the effect of three-body forces.

2.952 Å, and the hydrogen bond strength (dissociation energy) of $(H_2O)_2$ is 3.09 kcal/mol, corresponding to the zero-point-corrected binding energy (D_e) of 4.85 kcal/mol. The dimer equilibrium structure was determined in the potential surface fit described below, wherein a very extensive data set encompassing five of the six fundamental intermolecular vibrations with complete resolution of rotation and hydrogen bond tunneling effects, have been fit to Stone's highly detailed anisotropic site potential (ASP) potential form (38). Three distinct quantum tunneling processes (Fig. 4), for which the potential barriers all have been determined, rearrange the H-bond on time scales ranging from about 1 μs to 1 ps (38). The tunneling motions connect eight degenerate minima on the intermolecular potential surface (IPS), splitting each rovibrational transition into six subbands. The highest barrier (1.13 kcal/mol, zero point corrected) process corresponds to the exchange of the bound and free hydrogen atoms on the donor molecule (bifurcation) and turns out to be the most facile means of breaking the H-bond, which has interesting implications with respect to bond-breaking dynamics in bulk water (5, 41). All six fundamental intermolecular vibrations except for the out-of-plane libration have now been measured for both $(H_2O)_2$ and $(D_2O)_2$.

The water trimer is a much more rigid structure than the dimer (42), bound by three strained H-bonds (Fig. 5). The O—O distance in the trimer is 2.85 Å, significantly shorter than in the dimer, a result of the increased hydrogen bond strength caused by the cooperative effect of three-body forces. The appearance of three-body forces make inclusion of trimer VRT data into a fit of existing water pair potentials like VRT(ASP-W) the next logical step toward developing an accurate liquid water potential. The initial fits of potentials to the torsional energy levels below 100 cm^{-1}, as recently explored by Groenenboom *et al.* (39), will be followed by inclusion of the higher energy translational and librational vibrations, pending development of theoretical methods for treating such high-dimensional dynamics in clusters. The trimer VRT data therefore will allow explicit quantification of the three-body forces, the leading many-body term in the liquid force field.

Each monomer in the water trimer acts both as a single donor and single acceptor of an H-bond, and each has one bound and one free hydrogen. Because of the alternation of the free hydrogen atoms above and below the plane of the oxygens, this structure is chiral, as are those of all the odd-membered rings. Two distinct tunneling processes operate to rearrange the H-bond network, here connecting 48 degenerate minima on the IPS (43, 44). The first is flipping, which is essentially barrierless (Fig. 6*a*) (45), and the same bifurcation process described above for the dimer (Fig. 6*b*). This latter motion turns out to be a highly local one, with an uncorrected barrier near 2 kcal/mol(43, 44). These rearrangement pathways were systematically described in

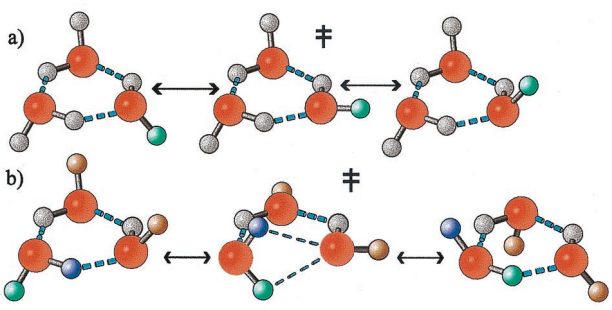

Fig. 6. Two distinct tunneling pathways rearrange the hydrogen bond pattern in the cyclic water trimer. The torsional (flipping) motion (*a*) of the free hydrogens atoms from one side of the plane determined by the oxygen atoms to the opposing side connects two degenerate minima on the IPS. The barrier for this tunneling motion is lower than the vibrational zero-point energy for $(H_2O)_3$ and close to the vibrational zero-point energy for $(D_2O)_3$ (43, 44, 104). Inclusion of flipping of all free hydrogens splits each torsional energy level into a manifold of six states. This flipping motion is symmetrically equivalent to rotation around the axis and hence is a pseudorotational motion coupling strongly to the overall rotation of the cluster, which results in severe Coriolis perturbations that can be readily observed in all torsional bands. Development of a detailed Hamiltonian accounting for this coupling was necessary for a complete understanding of the torsional states and analysis of the torsional bands (42). The bifurcation tunneling motion (*b*) in the water trimer consists of the exchange of a free and a bound hydrogen together with the flipping motion of the free hydrogens on the two neighboring water monomers. The bifurcation tunneling pathway is the lowest energy hydrogen bond breaking motion observed in water clusters, and, in the trimer, connects eight degenerate minima on the IPS, splitting each rovibrational transition into a quartet with relative intensities determined by the nuclear spin statistics. The barrier for this tunneling motion is about 2 kcal/mol and thus results in much smaller splittings than does the torsional tunneling motion (43, 45).

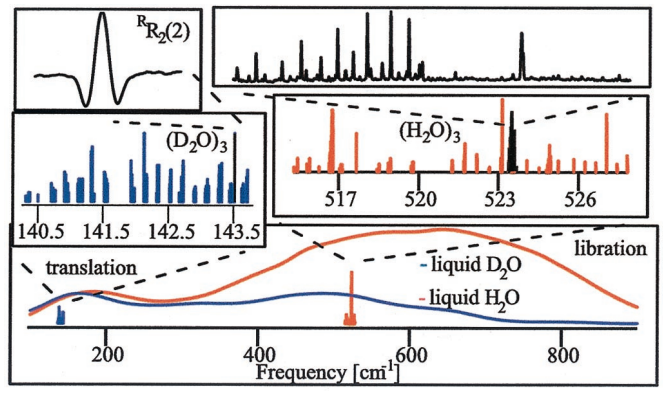

Fig. 7. The FIR spectrum of liquid D_2O and H_2O are shown together with the D_2O and H_2O cluster data in the translational (100–200 cm^{-1}) and librational (300–1,000 cm^{-1}) band region. (*Center Left*) A stick spectrum of the 142.8 cm^{-1} degenerate antisymmetric stretch band of $(D_2O)_3$. (*Top Left*) A scan of the $^RR_2(2)$ transition, representative of the strongest observed rovibrational transitions. The 142.8 cm^{-1} band lies well within the translational band of the liquid. No bifurcation tunneling splittings are observed, indicating that they are unchanged with respect to the ground state. (*Center Right*) The out-of-plane librational band of $(H_2O)_3$. Three parallel bands of $(H_2O)_3$ centered at 517.2, 523.9, and 525.3 cm^{-1} were assigned. Theory predicts only one parallel trimer band for the whole librational band region. The subbands were explained by a dramatic (×1,000) increase of tunneling splitting through the bifurcation pathway. (*Top Right*) A scan of the Q-branch of the 523.9 cm^{-1} subband is shown and from the observed relative intensities the rotational temperature can be estimated at 5 K.

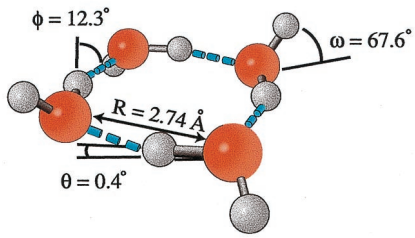

Fig. 8. The water tetramer has a highly symmetric homodromic S_4 equilibrium structure resulting in oblate symmetric top spectra with no vibrational averaging required. The symmetric structure requires highly concerted tunneling motions and results in a significantly more rigid structure than for the water trimer. The effect of many-body forces reduces the vibrationally averaged O—O distance from that of the trimer to 2.79 Å (2.74-Å *ab initio* equilibrium value) (105). The hydrogen bond is only 12° from linearity and the structure is very nearly planar.

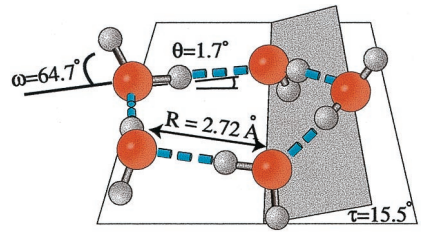

Fig. 10. The chiral homodromic equilibrium structure of the water pentamer is analogous to that of the water trimer. The vibrationally averaged O—O distance is 2.76 Å [2.72-Å equilibrium value from *ab initio* (54)], and the ring is puckered by 15.5°. The O—O—O angles are about 108°, very near the tetrahedral angle preferred in aqueous hydrogen bonding, and yielding nearly linear hydrogen bonds. As in the trimer, this structure also allows for very facile torsional motion and tunneling, connecting ten degenerate minima on the IPS. However, the torsional manifold resulting from this tunneling motion is more closely spaced, as coupling to the ring puckering motions is required. The hydrogen bond strength is larger than in the trimer and, thus, the bifurcation tunneling splitting, which connects 32 degenerate minima on the IPS, is reduced, and is only observable in $(H_2O)_5$ (Fig. 11).

elegant work by Walsh and Wales (44). The water trimer VRT data set is the most extensive existing for any water cluster, with seven, four, and six complete intermolecular vibrational bands observed for $(D_2O)_3$, $(H_2O)_3$, and mixed isotopomers, respectively. We have now achieved a very complete description of the low-frequency (<100 cm^{-1}) torsional modes in the trimer (42, 46, 47), and have measured extensive VRT spectra in the translational (26) (about 150 cm^{-1}, Fig. 7) and librational (27) (about 520 cm^{-1}, Fig. 7) band regions as well. Thus, all of the features of liquid water that appear in the intermolecular vibrational region ($\lambda > 10$ μm) also exist for the trimer and have been quite well characterized.

The H-bonding motif of the water tetramer is similar to that of the trimer, with each monomer acting as a single donor and acceptor, and having one free and one bound H (Fig. 8). The average O—O distance is further shortened to 2.79 Å. Interestingly, the water tetramer turns out to be more difficult to characterize than the trimer, as a result of its higher (S_4) symmetry (19, 24, 48, 49). Whereas the torsional motion of the free hydrogens in the trimer is very facile and results in a large number of low-frequency vibrational bands (<100 cm^{-1}), the only intermolecular vibration of the tetramer observed below 100 cm^{-1} both in $(D_2O)_4$ and $(H_2O)_4$ corresponds to the in-plane ring deformation. The lowest frequency vibrational band involving torsional states was observed at 137.8 cm^{-1} in $(D_2O)_4$ compared with the lowest torsional state of $(D_2O)_3$ at 8.5 cm^{-1}. The high symmetry also enforces much more cooperative tunneling motions, and the bifurcation rearrangement has not been observed. Rather, each vibration-rotation line is split into a doublet in a complicated tunneling process connecting only two degenerate minima on the tetramer IPS (49, 50), probably involving a second-order saddle point (Fig. 9).

The pentamer continues this structural evolution, being very similar to the trimer in both structure and dynamics (Fig. 10) (20, 22, 51, 52). Both torsional (flipping) and bifurcation tunneling are observed, connecting 320 degenerate minima on the IPS, but the time scale of both tunneling motions is slower than in the trimer. In contrast to the trimer, splittings due to bifurcation tunneling have been observed only for $(H_2O)_5$ and not $(D_2O)_5$, due to both the stronger H-bond and stronger coupling of flipping and ring puckering motion in the latter (52, 53). This coupling also requires heavy atom motion for the torsional motions and results in a much denser torsional manifold and a large number of dipole-allowed transitions at low frequencies (54). Many such transitions have been measured for the pentamer (Fig. 11), and the characterization of this torsional manifold is nearing completion (20, 22, 51, 55, 56).

The H-bond in the pentamer is nearly linear and the O—O distance of 2.76 Å is close to the value found for liquid water and especially ice, as the desired tetrahedral hydrogen bonding geometry of the monomers is very nearly realized. Moreover, molecular dynamics simulations have shown that five-membered rings are a dominant topology in liquid water, and pentamer-like patterns have

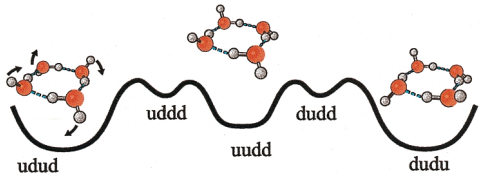

Fig. 9. The high symmetry of the tetramer requires highly concerted tunneling motions and limits the number of degenerate minima that can be connected on the IPS via feasible tunneling motions to two. The tunneling pathway connects the udud (up-down-up-down) structure with the dudu (down-up-down-up) one. Despite the small number of minima involved (trimer and pentamer 48 and 320 minima, respectively), the details of the tunneling pathway have been unclear. The observation of the large increase in tunneling splitting on exciting the 137.8 cm^{-1} e_g torsional vibration together with the analysis of the nuclear displacements derived by theory from this vibration suggests a complicated pathway involving sequential torsional motions of the free hydrogen/deuterium atoms and tunneling via second-order saddlepoints (49).

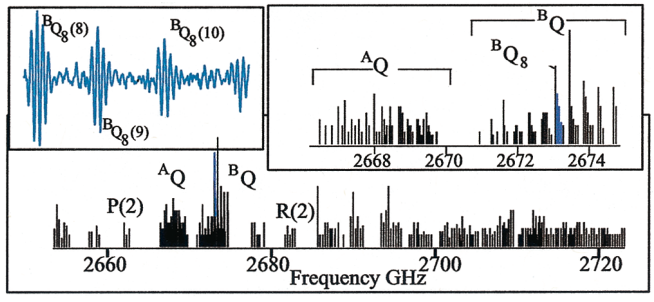

Fig. 11. The 89.1 cm^{-1} band of $(H_2O)_5$ is typical for a parallel band of an oblate symmetric top with first-order Coriolis perturbations into two subbands (A, B). Bifurcation tunneling splits each transition by 4.6 MHz into an equally spaced multiplet with a characteristic intensity pattern, determined by nuclear spin statistics. In contrast, the rovibrational transitions of the 81.1 cm^{-1} band of $(D_2O)_5$, show no sign of splittings due to bifurcation tunneling because of the larger mass involved.

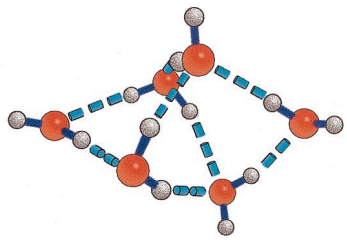

Fig. 12. The water hexamer has been determined to have a cage structure with the oxygens forming a distorted octahedron. The two apical water monomers are single donors and acceptors, whereas two of the other water monomers act as single donors, double acceptors and the remaining two as double donors, single acceptors. Bifurcation tunneling exchanges the free and bound hydrogens of the two apical water monomers, connecting four degenerate minima on the IPS. Calculations indicate that this cage form is the lowest of five low energy structures (21). A cyclic hexamer form, similar to that of the pentamer, recently has been identified in a liquid He droplet environment (57).

been shown to be important in solvation of hydrophobic solutes and in the structures of clathrate hydrates (95).

The hexamer represents the transition of the H-bond network from two-dimensional to three-dimensional in its most stable arrangement (Fig. 12). Here four monomers become triply H-bonded, whereas the two apical monomers remain doubly bonded in a nearly octahedral cage structure. These latter monomers engage in a cooperative type of bifurcation rearrangement, again enforced by the symmetry of the hydrogen bond network, and experimentally, tunneling between only two degenerate minima on the IPS is observed. It is notable that the most stable structure of the water hexamer determined in the gas phase resembles the basic unit in ice VI. Nauta and Miller (57) recently determined a cyclic structure of the hexamer in liquid helium droplets, analogous to those of the smaller clusters. Interestingly, this structure closely resembles the six membered ring forms existing in crystalline ice forms of water.

Although high-resolution experiments have not yet been successful for clusters larger than the hexamer $(H_2O)_n$, clusters with $n = 7, 8, 9, 10$ have been observed in low-resolution IR depletion experiments of size-selected clusters (58–60). The structures of these clusters were determined by comparing the experimental vibrational frequencies with the results of *ab initio* calculations for various structures. This analysis suggested the existence of both the D_{2d} and S_4 structures of the octamer, both of which correspond to stacked tetramer rings. Two heptamer structures derived from the S_4 octamer structure by removing one of the monomers also were determined, as well as a nonamer structure, expanding the D_{2d} cube structure of the octamer, which is composed of pentamer and tetramer units, and a decamer structure resembling the D_{2d} octamer structure with the two additional water molecules inserted at opposite edges.

Zwier and coworkers' (61, 62) resonant two-photon ionization, UV hole-burning, and resonant ion-dip IR spectroscopy studies also have suggested the existence of the two isomers of the octamer attached to benzene, which acts as a chromophore. Similarly, the structure of the water nonamer attached to a benzene chromophore was proposed to consist of an expanded octamer D_{2d} structure, whereas the existence of additional nonamer structures based on the S_4 octamer structure could not be determined definitively (63).

Toward a Universal Water Force Field from VRT Spectra

Theoretical calculations have clearly established the rapid convergence of the liquid water force field in terms of N-body interactions. Moreover, the leading nonpairwise additive term has been shown to be the relatively simple polarization (induction) interaction (64). It is therefore apparent that the essential information needed to deduce a quantitatively accurate liquid water force field can be extracted from appropriately detailed measurements of small water clusters, particularly dimer and trimer. In contrast to the results of water cluster studies in bulk environments, FIR VRT spectroscopy has been shown to provide such a probe (65), being exquisitely sensitive to the detailed topology of the cluster potential energy surface. Extensive VRT data sets now exist for several isotopomers of the dimer (66, 67) and trimer (25–27, 42, 46), encompassing all three types (torsion, translation, libration) of intermolecular vibrations of the trimer, and excluding only librations in the dimer (66, 67), whereas somewhat less data exist for the water tetramer, pentamer, and hexamer. Hence, given the requisite theoretical methods for computing cluster VRT spectra from global potential surfaces, we now have the capability to actually construct a rigorously accurate force field for liquid water from the spectra of these small clusters.

The first step in our scheme to accomplish this goal is to rigorously determine the water dimer potential energy surface by explicitly fitting the VRT data to a detailed and physically sound potential model. This dimer potential surface will accurately describe not only the dominant pairwise interactions that occur in the liquid, but if it properly includes both electric multipoles and polarizibility of the water molecule, then it will also correctly describe the leading nonadditive terms, namely N-body induction. Hence, an approximate potential surface of the trimer can be constructed by appropriate summation of the polarizable dimer potential (treating the induction by iteration or matrix inversion). The interactions not properly described by this potential [three-body exchange and the much smaller (64) three-body dispersion] then can be quantified by comparing VRT spectra of the trimer with those computed from the potential surface. This process can be extended and refined by successively addressing the larger clusters (tetramer, pentamer, and hexamer) in the same way. We suggest that a potential that rigorously describes the VRT spectra of the trimer will already accurately reproduce the measured properties of liquid water over large ranges of conditions, thereby essentially providing the long-sought universal water force field.

This first step outlined above (determination of the dimer potential) has now been accomplished. A key development in this process was the Split Wigner Pseudospectral method (68) and its implementation for the water dimer (69, 70). This theoretical advance permitted the accurate computation of dimer eigenstates from van der Avoird's rigorously derived body-fixed six-dimensional scattering Hamiltonian (71) and a suitable global potential surface with the very high efficiency and economy required for incorporation of this procedure into a regression routine. Two water dimer potential surfaces of spectroscopic accuracy have now been published. Fellers *et al.* (38) fit the dimer VRT data to Millot and Stone's ASP-W potential (72), the most detailed dimer surface available, and van der Avoird and colleagues (39, 73, 74) "tuned" the *ab initio* symmetry adapted perturbation theory (SAPT) surface of Mas and Szalewicz (7) to reproduce these same data. The quality of these two potential surfaces is comparable, as judged by their respective abilities to reproduce the VRT data and the temperature dependence of the second virial coefficients. Both are far more accurate than any of the many water dimer potentials previously available (69, 70). Perhaps their most notable feature is the significantly reduced dimer binding energy (4.85–5.00 kcal/mol), in accord with the latest *ab initio* results (6, 7).

Perhaps surprisingly, we now recognize that the key ingredient for constructing a rigorously accurate liquid water force field is actually this dimer potential surface. Accordingly, we must seek to obtain the "perfect" dimer potential. Although the two new forms obtained from VRT data are certainly dramatic improve-

ments, they both have flaws. The VRT(ASP-W) surface is weakest in its description of the acceptor switching tunneling motion, yielding a trimer flipping barrier that is too high. The symmetry adapted perturbation theory (SAPT) potential is not explicitly polarizable, and therefore cannot be used in its present form to construct potentials for either larger clusters or bulk water. Both potentials are constructed with "frozen monomers," and thus do not produce the slight elongation of the covalent O—H bond that is known to occur in the donor of the H-bond. The relaxation of the monomer rigidity constraint may be necessary to improve these features. However, this necessitates rigorously solving a 12-dimensional vibrational dynamics Hamiltonian, something not considered even remotely possible until very recently.

Leforestier *et al.* (C. Leforestier, N. Goldman, C. Keoshian, L. B. Braly, and R.J.S., unpublished work) recently performed a least-squares fit of H_2O dimer VRT data to a 12-dimensional potential, which uses the H_2O monomer potential recently developed by Polyanski *et al.* (76) to describe the covalent bond vibrations, and a modified Matsuoka Clementi Yoshimine (MCY) potential form of Clementi and coworkers (77) for the intermolecular interactions. The eigenstates of the 12-dimensional potential were computed by the Split Wegner Pseudospectral (SWPS) method, but incorporating an adiabatic separation between the covalent and intermolecular motions. Interestingly, this very simple MCY potential (11 free parameters) fits the VRT data quite well, but only when the intramolecular nonrigidity is included (but with no additional free parameters); the modified MCY potential performed rather badly when only six-dimensional dynamics (rigid monomers) were calculated (69, 70, 78).

The Berkeley/Nijmegen collaboration has achieved a complete characterization of the trimer VRT states in the torsional (pseudorotational) manifold for both H_2O and D_2O isotopes (42, 46), first treated theoretically by Schütz *et al.* (79). Van der Avoird *et al.* (80) have derived a rigorous body-fixed Hamiltonian for these motions, treating the three torsional motions explicitly (fully coupled) and the librational (bifurcation) motions perturbatively, while freezing the translational vibrations. The Berkeley group (42, 46) has accomplished a global fit of all of the torsional VRT data to this Hamiltonian. Groenenboom *et al.* (39) have subsequently used these states to check the "tuning" of their symmetry adapted perturbation theory (SAPT)-5st potential, finding an impressive level of agreement (39). Keutsch *et al.* have very recently characterized both the translational (26) and librational (27) vibrations in the trimer by VRT spectroscopy, and Sabo *et al.* (81) have developed a four-dimensional trimer model incorporating the effects of the symmetric translational mode on the torsional states. Hence, the stage is set for carrying out the refinement of the pair potential and the rigorous determination of the three-body corrections, pending some further development of the requisite theoretical formalism (to describe the coupling of translation, torsion, and libration in the rotating frame—another difficult 12-dimensional dynamics problem).

Dynamics of the Hydrogen Bond in Water Clusters

Although the determination of an accurate potential for liquid water has thus far been the main goal of the FIR-VRT water cluster studies, we recently have sought to exploit the molecular details of structures and hydrogen bond dynamics revealed in our VRT spectroscopy experiments to elucidate specific aspects of these dynamics occurring in the liquid (21, 49, 51, 55, 82). The hydrogen bond network and its dynamics determine the unique properties of liquid water, and many different experiments have addressed these in terms of the underlying intermolecular motions (83–91). In contrast to the VRT experiments, these bulk experiments were either insensitive to the microscopic details or required extensive interpretation (92). In conjunction with interpretation by theoretical models, the experimental results have suggested that both the translational (hydrogen bond stretch vibration centered at 180 cm^{-1} in H_2O) and the librational motions (hindered rotational vibration about 300–1,000 cm^{-1} H_2O) are directly involved in most dynamical processes (5, 85, 86, 89, 92–96).

The free hydrogens in small water clusters—the main distinction between clusters and the bulk—are predicted not to influence these two important intermolecular motions (translation and libration) significantly (ref. 97 and A. Luzar, personal communication). Although water clusters are certainly not important as isolated constituents of liquid water and clearly cannot act as models of long time dynamics (e.g., diffusion), we have investigated by using water clusters to unravel the details of hydrogen bond dynamics on very short time scales, specifically the hydrogen bond breaking dynamics (41). Chandler and Luzar (5, 92) have studied this aspect of the liquid dynamics via computer simulations, and their results imply that these dynamics are primarily local and do not vary significantly with the hydrogen bond order in the liquid. Their studies, in conjunction with the above experiments, also suggest that librational motions play the central role in liquid-state dynamics because they are the dominant motion for the initial breaking of hydrogen bonds in the extended network. Whereas translational motions themselves do not lead to significant bond breaking, they can indirectly facilitate the breaking by weakening the hydrogen bond (5, 91, 92, 95, 99). The interpretation of recent dielectric relaxation measurements has even suggested that water molecules making only two hydrogen bonds might be of special importance for bulk dynamics (88). These results therefore suggest that water clusters can indeed provide a paradigm for elucidating the molecular details of specific local processes contributing to the liquid-state dynamics, namely the hydrogen bond breaking, despite the obvious disparities.

Water cluster VRT experiments do not contain dynamical information *per se*, as they measure transitions between stationary states. However, the magnitude of the tunneling splittings observed for a specific vibrational state characterize the feasible hydrogen bond rearrangements in the cluster. It is straightforward to extract a time scale for a given tunneling motion from the experimental splittings (100, 101), and thus the time scale for the hydrogen bond dynamics associated with a tunneling pathway can be determined. This time scale calculation allows a direct study of the effect of exciting specific intermolecular motions (e.g., translation and libration) on the dynamics for various cluster sizes.

The bifurcation pathway (Fig. 6*b*) is uniquely suited for the study of the dynamics of the hydrogen bond in small water clusters, as it has been observed for the dimer, trimer, pentamer, and hexamer (49, 51), and corresponds to the lowest energy pathway for breaking and making a hydrogen bond, precisely the aspect of the liquid-state dynamics we are interested in. Furthermore, the potential barrier for the bifurcation pathway is similar for all water clusters studied so far and it is a local process (49, 51), hence we can use this specific tunneling process as a probe of the hydrogen bond breaking dynamics and investigate the effect of both cluster size and excitation of various intermolecular vibrations on these bifurcation dynamics. From the experimentally determined magnitude of the bifurcation tunneling splitting for a given vibrational state, we can extract the time scale for breaking and making a hydrogen bond—i.e., the hydrogen bond lifetime (τ_H) of that state. Presently, the water trimer is the only water cluster for which all classes of intermolecular vibrations have been observed, allowing the first study of intermolecular vibrational mode selectivity on the hydrogen bond lifetime, and the determination of the dominant intermolecular hydrogen bond breaking motion.

From a vibrational ground state splitting of about 0.0033 cm^{-1} the hydrogen bond lifetime of the ground state was determined to be $\tau_H(GS) = 1–2$ ns for $(H_2O)_3$ (101). The very small variation of the magnitude of the tunneling splitting among states examined in the torsional manifold confirms that the hydrogen bond lifetime does not change significantly upon excitation of torsional vibrations, $\tau_H(\text{torsion}) \approx 1–2$ ns for $(H_2O)_3$ (101). The first observed translational vibration of a water cluster, the 142.8 cm^{-1} $(D_2O)_3$ band (Fig. 7), showed no evidence of bifurcation tunneling splittings within the experimental uncertainty (about 2 MHz) (26). Therefore, the magnitude of these tunneling splitting and, thus, the hydrogen bond lifetime for the excited state has to be nearly identical upon exciting the translational vibration, $\tau_H(\text{translation}) \approx \tau_H(GS) = 1–2$ ns for $(H_2O)_3$. Our recent study of the librational band region revealed three parallel bands of $(H_2O)_3$ at 517.2, 523.9, and 525.3 cm^{-1} (Fig. 7), which are located close to the center of the librational band of liquid H_2O and are assigned to the out-of-plane libration (27). The splittings for the excited state of the libration are so large that the three individual bands observed within 8 cm^{-1} correspond to the tunneling components, revealing that the bifurcation splittings are nearly 3 orders of magnitude larger than for the vibrational ground state. Although the calculation of the hydrogen bond lifetime is more complicated for the excited state of the out-of-plane libration as the high barrier limit for the tunneling pathway is no longer valid, we can extract a hydrogen bond lifetime of $\tau_H(\text{libration}) = 1–6$ ps.

This time scale is strikingly similar to the accepted average hydrogen bond lifetime found in liquid water (≈1 ps), and the time scales of a number of important dynamical processes in bulk phases of water, (attributed to single molecule reorientation) e.g., dielectric relaxation ($\tau_D \approx 8–9$ ps, $\tau_{D2} \approx 1$ ps) (93), reorientation relaxation ($\tau_1 \approx 13$ ps, $\tau_2 \approx 0.7$ ps) (90) and proton mobility (≈1 ps) (93). Whereas the molecular details of the tunneling motions and vibrations we observe in small water clusters are well understood (43, 44, 102), none of the experiments used for measuring these bulk time scales are sensitive to the microscopic details, and accordingly any molecular interpretation of these results on the bulk is necessarily strongly model-dependent. The value of the VRT results is that they clearly demonstrate the dramatic effect of exciting specific intermolecular motions on the hydrogen bond breaking rate, with the librations clearly being the dominant intermolecular hydrogen bond breaking motion. Therefore, rather than the perhaps coincidental similarities of τ_H(libration) with those of the bulk relaxation processes, the most important result of our study is that we have confirmed the same dependence of the hydrogen bond breaking dynamics on intermolecular motions in the water trimer as postulated in theoretical studies of liquid water. Specifically, we observe a dramatic increase (×1,000) in the rate of hydrogen bond breaking compared with that in the ground state of the water trimer upon excitation of a single quantum in the librational mode, no change of τ_H upon single quantum excitation of a translational mode, and an insignificant change of τ_H on excitation of the torsional vibrations. Hence, libration is the dominant vehicle for breaking and making the hydrogen bond, just as postulated to be the case for liquid water.

This work was supported mainly by the Experimental Physical Chemistry Program of the National Science Foundation. The Berkeley cavity ringdown laser absorption spectrometry effort also was supported by the Chemical Dynamics Program of the Air Force Office of Scientific Research.

1. Stillinger, F. H. (1980) *Science* **209,** 451–457.
2. Chen, B., Xing, J. & Siepmann, J. I. (2000) *J. Phys. Chem.* **104,** 2391–2401.
3. Makkonen, L. (1997) *J. Phys. Chem.* **101,** 6196–6200.
4. Harrington, S., Zhang, R., Poole, P. H., Sciortino, F. & Stanley, H. E. (1997) *Phys. Rev. Lett.* **78,** 2409–2412.
5. Luzar, A. & Chandler, D. (1996) *Phys. Rev. Lett.* **76,** 928–931.
6. Stone, A. J. (1996) *The Theory of Intermolecular Forces* (Oxford Univ. Press, Oxford).
7. Mas, E. M. & Szalewicz, K. (1996) *J. Chem. Phys.* **104,** 7606–7614.
8. Silvestrelli, P. L. & Parrinello, M. (1999) *J. Chem. Phys.* **111,** 3572–3580.
9. Busarow, K. L., Cohen, R. C., Blake, G. A., Laughlin, K. B., Lee, Y. T. & Saykally, R. J. (1989) *J. Chem. Phys.* **90,** 3937–3943.
10. Dyke, T. R., Mack, K. M. & Muenter, J. S. (1977) *J. Chem. Phys.* **66,** 498–510.
11. Fraser, G. T. (1991) *Int. Rev. Phys. Chem.* **10,** 189–206.
12. Zwart, E., Termeulen, J. J., Meerts, W. L. & Coudert, L. H. (1991) *J. Mol. Spectrosc.* **147,** 27–39.
13. Pugliano, N. & Saykally, R. J. (1992) *Science* **257,** 1937–1940.
14. Blake, G. A., Laughlin, K. B., Cohen, R. C., Busarow, K. L., Gwo, D. H., Schmuttenmaer, C. A., Steyert, D. W. & Saykally, R. J. (1991) *Rev. Sci. Instr.* **62,** 1693–1700.
15. Blake, G. A., Laughlin, K. B., Cohen, R. C., Busarow, K. L., Gwo, D. H., Schmuttenmaer, C. A., Steyert, D. W. & Saykally, R. J. (1991) *Rev. Sci. Instr.* **62,** 1701–1716.
16. Liu, K., Fellers, R. S., Viant, M. R., McLaughlin, R. P., Brown, M. G. & Saykally, R. J. (1996) *Rev. Sci. Instr.* **67,** 410–416.
17. Pugliano, N., Cruzan, J. D., Loeser, J. G. & Saykally, R. J. (1993) *J. Chem. Phys.* **98,** 6600–6617.
18. Liu, K., Elrod, M. J., Loeser, J. G., Cruzan, J. D., Pugliano, N., Brown, M. G., Rzepiela, J. & Saykally, R. J. (1994) *Faraday Discuss. Chem. Soc.* **94,** 35–41.
19. Cruzan, J. D., Braly, L. B., Liu, K., Brown, M. G., Loeser, J. G. & Saykally, R. J. (1996) *Science* **271,** 59–62.
20. Liu, K., Brown, M. G., Cruzan, J. D. & Saykally, R. J. (1996) *Science* **271,** 62–64.
21. Liu, K., Brown, M. G., Carter, C., Saykally, R. J., Gregory, J. K. & Clary, D. C. (1996) *Nature (London)* **381,** 501–503.
22. Liu, K., Brown, M. G., Cruzan, J. D. & Saykally, R. J. (1997) *J. Phys. Chem.* **101,** 9011–9021.
23. Liu, K., Brown, M. G. & Saykally, R. J. (1997) *J. Phys. Chem.* **101,** 8995–9010.
24. Cruzan, J. D., Viant, M. R., Brown, M. G. & Saykally, R. J. (1997) *J. Phys. Chem.* **101,** 9022–9031.
25. Viant, M. R., Cruzan, J. D., Lucas, D. D., Brown, M. G., Liu, K. & Saykally, R. J. (1997) *J. Phys. Chem.* **101,** 9032–9041.
26. Keutsch, F. N., Brown, M. G., Petersen, P. B., Saykally, R. J., Geleijns, M. & van der Avoird, A. (2000) *J. Chem. Phys.* **114,** 3934–4004.
27. Keutsch, F. N., Fellers, R., Viant, M. R. & Saykally, R. J. (2000) *J. Chem. Phys.* **114,** 4005–4015.
28. van Thiel, M., Becker, E. D. & Pimentel, G. C. (1957) *J. Chem. Phys.* **27,** 486–490.
29. Vernon, M. F., Lisy, J. M., Krajnovich, D. J., Tramer, A., Hoi-Sing, K., Ron Shen, Y. & Lee, Y. T. (1982) *Faraday Discuss. Chem. Soc.* **73,** 387–397.
30. Page, R. H., Frey, J. G., Shen, Y. R. & Lee, Y. T. (1984) *Chem. Phys. Lett.* **106,** 373–376.
31. Coker, D. F., Miller, R. E. & Watts, R. O. (1985) *J. Chem. Phys.* **82,** 3554–3562.
32. Huang, Z. S. & Miller, R. E. (1989) *J. Chem. Phys.* **91,** 6613–6631.
33. Huang, Z. S. & Miller, R. E. (1988) *J. Chem. Phys.* **88,** 8008–8009.
34. Frochtenicht, R., Kaloudis, M., Koch, M. & Huisken, F. (1996) *J. Chem. Phys.* **105,** 6128–6140.
35. Paul, J. B., Provencal, R. A., Chapo, C., Roth, K., Casaes, R. & Saykally, R. J. (1999) *J. Phys. Chem.* **103,** 2972–2974.
36. Paul, J. B., Provencal, R. A. & Saykally, R. J. (1998) *J. Phys. Chem.* **102,** 3279–3283.
37. Paul, J. B., Provencal, R. A., Chapo, C., Petterson, A. & Saykally, R. J. (1998) *J. Chem. Phys.* **109,** 10201–10206.
38. Fellers, R. S., Leforestier, C., Braly, L. B. & Brown, M. G. (1999) *Science* **284,** 945–948.
39. Groenenboom, G. C., Mas, E. M., Bukowski, R., Szalewicz, K., Wormer, P. E. S. & van der Avoird, A. (2000) *Phys. Rev. Lett.* **84,** 4072–4075.
40. Paul, J. B., Collier, C. P., Saykally, R. J., Scherer, J. J. & O'Keefe, A. (1997) *J. Phys. Chem.* **101,** 5211–5214.
41. Keutsch, F. N., Fellers, R. S., Brown, M. G., Viant, M. R., Petersen, P. B. & Saykally, R. J. (2001) *J. Am. Chem. Soc.* **123,** 5938–5941.
42. Viant, M. R., Brown, M. G., Cruzan, J. D., Saykally, R. J., Geleijns, M. & van der Avoird, A. (1999) *J. Chem. Phys.* **110,** 4369–4381.
43. Wales, D. J. (1993) *J. Am. Chem. Soc.* **115,** 11180–11190.
44. Walsh, T. R. & Wales, D. J. (1996) *J. Chem. Soc. Faraday Trans.* **92,** 2505–2517.
45. Fowler, J. E. & Schaefer, H. F. (1995) *J. Am. Chem. Soc.* **117,** 446–452.
46. Brown, M. G., Viant, M. R., McLaughlin, R. P., Keoshian, C. J., Michael, E., Cruzan, J. D., Saykally, R. J., Geleijns, M. & van der Avoird, A. (1999) *J. Chem. Phys.* **111,** 7789–7800.
47. Keutsch, F. N., Karyakin, E. N., Saykally, R. J. & van der Avoird, A. (2000) *J. Chem. Phys.* **114,** 3988–3933.

48. Cruzan, J. D., Brown, M. G., Liu, K., Braly, L. B. & Saykally, R. J. (1996) *J. Chem. Phys.* **105,** 6634–6644.
49. Brown, M. G., Keutsch, F. N., Braly, L. B. & Saykally, R. J. (1999) *J. Chem. Phys.* **111,** 7801–7806.
50. Wales, D. J. & Walsh, T. R. (1997) *J. Chem. Phys.* **106,** 7193–7207.
51. Brown, M. G., Keutsch, F. N. & Saykally, R. J. (1998) *J. Chem. Phys.* **109,** 9645–9647.
52. Wales, D. J. & Walsh, T. R. (1996) *J. Chem. Phys.* **105,** 6957–6971.
53. Gregory, J. K. & Clary, D. C. (1996) *J. Chem. Phys.* **105,** 6626–6633.
54. Graf, S., Mohr, W. & Leutwyler, S. (1999) *J. Chem. Phys.* **110,** 7893–7908.
55. Liu, K., Cruzan, J. D. & Saykally, R. J. (1996) *Science* **271,** 929–933.
56. Cruzan, J. D., Viant, M. G., Brown, M. G., Lucas, D. D., Kun, L. & Saykally, R. J. (1998) *Chem. Phys. Lett.* **292,** 667–676.
57. Nauta, K. & Miller, R. E. (2000) *Science* **287,** 293–295.
58. Sadlej, J., Buch, V., Kazimirski, J. K. & Buck, U. (1999) *J. Phys. Chem.* **103,** 4933–4947.
59. Brudermann, J., Melzer, M., Buck, U., Kazimirski, J. K., Sadlej, J. & Buch, V. (1999) *J. Chem. Phys.* **110,** 10649–10652.
60. Buck, U., Ettischer, I., Melzer, M., Buch, V. & Sadlej, J. (1998) *Phys. Rev. Lett.* **80,** 2578–2581.
61. Gruenloh, C. J., Carney, J. R., Hagemeister, F. C., Arrington, C. A., Zwier, T. S., Fredericks, S. Y., Wood, J. T., III & Jordan, K. D. (1998) *J. Chem. Phys.* **109,** 6601–6614.
62. Gruenloh, C., Carney, J., Arrington, C., Zwier, T., Fredericks, S. & Jordan, K. (1997) *Science* **276,** 1678–1681.
63. Gruenloh, C. J., Carney, J. R., Hagemeister, F. C., Zwier, T. S., Wood, J. T. & Jordan, K. D. (2000) *J. Chem. Phys.* **113,** 2290–2303.
64. Xantheas, S. S. (1994) *J. Chem. Phys.* **100,** 7523–7534.
65. Saykally, R. J. & Blake, G. A. (1993) *Science* **259,** 1570–1575.
66. Braly, L. B., Cruzan, J. D., Liu, K., Fellers, R. S. & Saykally, R. J. (2000) *J. Chem. Phys.* **112,** 10293–10313.
67. Braly, L. B., Liu, K., Brown, M. G., Keutsch, F. N., Fellers, R. S. & Saykally, R. J. (2000) *J. Chem. Phys.* **112,** 10314–10326.
68. Leforestier, C. (1994) *J. Chem. Phys.* **101,** 7357–7363.
69. Leforestier, C., Braly, L. B., Kun, L., Elrod, M. J. & Saykally, R. J. (1997) *J. Chem. Phys.* **106,** 8527–8544.
70. Fellers, R. S., Braly, L. B., Saykally, R. J. & Leforestier, C. (1999) *J. Chem. Phys.* **110,** 6306–6318.
71. Brocks, G., van der Avoird, A., Sutcliffe, B. T. & Tennyson, J. (1983) *Mol. Phys.* **60,** 1025–1043.
72. Millot, C. & Stone, A. J. (1992) *Mol. Phys.* **77,** 439–462.
73. Mas, E. M., Bukowski, R., Szalewicz, K., Groenenboom, G. C., Wormer, P. E. S. & van der Avoird, A. (2000) *J. Chem. Phys.* **113,** 6687–6701.
74. Groenenboom, G. C., Wormer, P. E. S., van der Avoird, A., Mas, E. M., Bukowski, R. & Szalewicz, K. (2000) *J. Chem. Phys.* **113,** 6702–6715.
75. Xantheas, S. S. & Dunning, T. H., Jr. (1993) *J. Chem. Phys.* **99,** 8774–8792.
76. Polyansky, O., Jensen, P. & Tennyson, J. (1996) *J. Chem. Phys.* **105,** 6490–6497.
77. Matsuoka, O., Clementi, E. & Yoshimine, M. (1976) *J. Chem. Phys.* **64,** 1351–1361.
78. Fellers, R. S. (1998) Ph.D. Thesis (Univ. of California, Berkeley).
79. Schutz, M., Burgi, T., Leutwyler, S. & Burgi, H. B. (1993) *J. Chem. Phys.* **99,** 5228–5238.
80. van der Avoird, A., Olthof, E. H. T. & Wormer, P. E. S. (1996) *J. Chem. Phys.* **105,** 8034–8050.
81. Sabo, D., Bacic, Z., Graf, S. & Leutwyler, S. (1999) *J. Chem. Phys.* **110,** 5745–5757.
82. Liu, K., Loeser, J. G., Elrod, M. J., Host, B. C., Rzepiela, J. A., Pugliano, N. & Saykally, R. J. (1994) *J. Am. Chem. Soc.* **116,** 3507–3512.
83. Draegert, D. A. & Williams, D. (1968) *J. Chem. Phys.* **48,** 401–407.
84. Ricci, M. A., Signorelli, G. & Mazzacurati, V. (1990) *J. Phys. Cond. Matt.* **2,** SA183–SA187.
85. Teixeira, J., Bellissent-Funel, M.-C. & Chen, S.-H. (1990) *J. Phys. Cond. Matt.* **2,** SA105–SA108.
86. Barthel, J., Bachhuber, K., Buchner, R. & Hetzenauer, H. (1990) *Chem. Phys. Lett.* **165,** 369–373.
87. Sastry, S., Stanley, H. E. & Sciortino, F. (1994) *J. Chem. Phys.* **100,** 5361–5366.
88. Buchner, R., Barthel, J. & Stabuer, J. (1999) *Chem. Phys. Lett.* **306,** 57–63.
89. Lang, M. J., Jordanides, X. J., Song, X. & Fleming, G. R. (1999) *J. Chem. Phys.* **110,** 5884–5892.
90. Woutersen, S., Emmerichs, U. & Bakker, H. J. (1997) *Science* **278,** 658–660.
91. Bakker, H. J., Woutersen, S. & Nienjuys, H. K. (2000) *Chem. Phys.* **258,** 233–245.
92. Luzar, A. & Chandler, D. (1996) *Nature (London)* **379,** 55–57.
93. Agmon, N. (1996) *J. Phys. Chem.* **100,** 1072–1080.
94. Chen, S.-H., Gallo, P., Sciortino, F. & Tartaglia, P. (1997) *Phys. Rev. E* **56,** 4231–4242.
95. Csajka, F. S. & Chandler, D. (1998) *J. Chem. Phys.* **109,** 1125–1133.
96. Schmitt, U. W. & Voth, G. A. (1999) *J. Chem. Phys.* **111,** 9361–9381.
97. Bosma, W. B., Fried, L. E. & Mukamel, S. (1993) *J. Chem. Phys.* **98,** 4413–4421.
98. Xantheas, S. S. & Dunning, T. H. (1993) *J. Chem. Phys.* **98,** 8037–8040.
99. Luzar, A. & Chandler, D. (1993) *J. Chem. Phys.* **98,** 8160–8173.
100. Feynman, R. P., Leighton, R. B. & Sands, M. (1964) in *The Feynman Lectures on Physics*, eds. Feynman, R. P., Leighton, R. B. & Sands, M. (Addison–Wesley, Reading), pp. 8-12–8-14.
101. Brown, M. G. (1999) Ph.D. Thesis (Univ. of California, Berkeley).
102. Olthof, E. H. T., van der Avoird, A., Wormer, P. E. S., Liu, K. & Saykally, R. J. (1996) *J. Chem. Phys.* **105,** 8051–8063.
103. Suzuki, S. & Blake, G. A. (1994) *Chem. Phys. Lett.* **229,** 499–505.
104. Klopper, W., Schutz, M., Luthi, H. P. & Leutwyler, S. (1995) *J. Chem. Phys.* **103,** 1085–1098.